ACS OMEGA

http://pubs.acs.org/journal/acsodf

Article

The Effect of Degrees of Inversion on the Electronic Structure of Spinel $NiCo_2O_4$: A Density Functional Theory Study

Tzu-Chien Chang,[#] Yi-Ting Lu,[#] Chih-Heng Lee, Jyoti K. Gupta, Laurence J. Hardwick, Chi-Chang Hu, and Hsin-Yi Tiffany Chen*

Cite This: https://doi.org/10.1021/acsomega.1c00295

Read Online

ACCESS | Metrics & More | Article Recommendations | Supporting Information

ABSTRACT: In this study, electronic structure calculations and Bader charge analysis have been completed on the inverse, intermediate, and normal spinel structures of $NiCo_2O_4$ in both primitive and conventional cells, using density functional theory with Hubbard U correction. Three spinel structures have been computed in the primitive cell, where the fully inverse spinel, 50% intermediate spinel, and normal spinel can be acquired by swapping Ni and Co atoms on tetrahedral and octahedral sites. Furthermore, $NiCo_2O_4$ with different degrees of inversion in the conventional cells was also investigated, along with their doping energies. Confirmed by the assigned formal charges, magnetic moments, and decomposed density of state, our results suggest that the electronic properties of Ni and Co on the tetrahedral site can be altered by swapping Ni and Co atoms, whereas both Ni and Co on the octahedral site are uninfluenced. A simple and widely used model, crystal field theory, is also compared with our calculations and shows a consistent prediction about the cation distribution in $NiCo_2O_4$. This study analyzes the correlation between cation arrangements and formal charges, which could potentially be used to predict the desired electronic properties of $NiCo_2O_4$ for various applications.

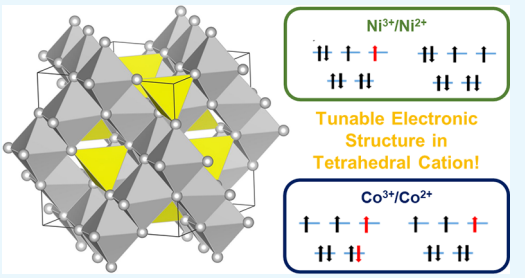

1. INTRODUCTION

$NiCo_2O_4$ is a widely used material, which has been studied in various fields, such as metal−air batteries,[1−5] supercapacitors,[6−8] electrochemical sensors,[9−11] water splitting,[12−14] and photocatalysis.[15−17] The presence of abundant redox couples (Ni^{2+}/Ni^{3+} and Co^{2+}/Co^{3+}) in $NiCo_2O_4$ can provide sufficient active sites, leading to a good electrochemical/catalytic performance.[18] For example, the Co^{2+} and Ni^{3+} cations are reported to be the active sites for the oxygen reduction reaction and oxygen evolution reaction.[5,19−23] These examples indicate the importance of cations that possess the desired oxidation state and thus can serve as the active sites for electrochemical/catalytic reactions.

The origin of the oxidation states of Ni and Co cations are therefore of great interest. A simple formula supported by X-ray absorption spectroscopy describes how Ni/Co cations with different charges are distributed in the tetrahedral (Td) and octahedral (Oh) sites:[24]

$$(Co_x^{2+}Co_{1-x}^{3+})_{Td}[Co^{3+}Ni_{1-x}^{2+}Ni_x^{3+}]_{Oh}O_4\ (0 \le x \le 1) \quad (1)$$

In this formula, Ni cations occupy octahedral sites, and Co cations are situated in both tetrahedral sites and octahedral sites. Although Ni cations are often reported to locate in the octahedral sites, some evidences point out that the exchange between tetrahedral Co and octahedral Ni takes place easily and frequently.[25,26] Taking into account the cation exchange, the formula of $NiCo_2O_4$ can be rewritten as follows:

$$(Co_xNi_{1-x})_{Td}[Co_{2-x}Ni_x]_{Oh}O_4\ (0 \le x \le 1) \quad (2)$$

where the fraction (x) of Ni in the octahedral site is referred to as the degree of inversion (DOI).[27] When DOI = 1 (i.e., x = 1) in formula (2), $NiCo_2O_4$ is in an inverse spinel configuration (as shown in Figure 1a). On the other hand, when DOI = 0 (x = 0), it is in a normal spinel configuration (shown in Figure

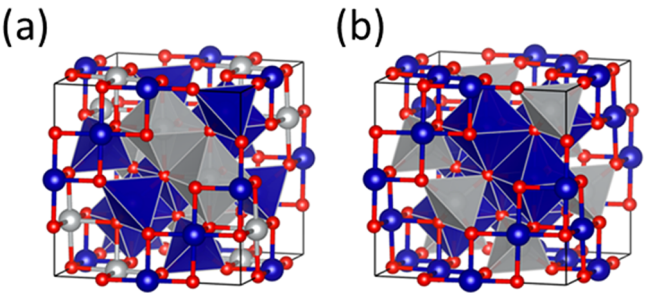

Figure 1. Crystal structure of (a) inverse and (b) normal spinel in a conventional unit cell. O atoms are shown in red, Ni atoms in gray, and Co atoms in blue.

Received: January 17, 2021
Accepted: March 12, 2021

1b). Except the inverse and normal structures, all other configurations are the intermediate structures that can be regarded as the combination of both inverse and normal structures with different ratios.

In the literature, many studies focused only on a pure inverse spinel structure of $NiCo_2O_4$,[28,29] despite the fact that intermediate structures are also likely to form, due to different synthesis processes.[27,30,31] Some groups reported studies on the intermediate states of a spinel structure. For example, Ndione *et al.* proposed that the electrical properties of $NiCo_2O_4$ and $ZnCo_2O_4$ can be controlled by manipulating the DOI,[27] and Dileep *et al.* reported on various band gaps for $NiCo_2O_4$ with three different cation configurations.[32] However, these works primarily focused on physical properties such as band gaps or electrical conductivities. Accordingly, the oxidation state of cations and its relationship with the structure of $NiCo_2O_4$ have not been fully elucidated.

Taking the above into consideration, the motivation of this study is to investigate the relationship between the DOI and physical properties (i.e., oxidation state, electronic structure, and band structure). With the aid of theoretical calculations, we have systematically investigated how the site distribution (tetrahedral or octahedral) affects the cation oxidation state, magnetic moment, and electronic structure of $NiCo_2O_4$ in the spinel structure by conducting density functional theory calculations on $NiCo_2O_4$ with the Hubbard U correction (DFT + U). The results show a clear relationship between the oxidation state of Ni/Co cations and cation configuration and suggest a possibility that the $NiCo_2O_4$ with desirable properties for a specific application can be obtained by changing the spinel configuration to some extent.

2. COMPUTATIONAL DETAILS

Spin-polarized density functional theory (DFT) calculations in this work were carried out using projector augmented wave (PAW) methods to describe the ion−electron interactions as implemented in Vienna Ab initio Simulation Package (VASP).[33,34] The valence electron configuration in the calculation was $3d^84s^2$ for Ni, $3d^74s^2$ for Co, and $2s^2p^4$ for O. Plane-wave expansion was truncated at a cut-off energy of 680 eV for primitive and conventional unit cells. Perdew−Burke−Ernzerhof (PBE) functional of the generalized gradient approximation (GGA) was adopted to describe the exchange and correlation effects.[35,36] Additionally, in order to correct for the strong correlation of 3d electrons in transition metals, a rotationally invariant Hubbard U correction proposed by Dudarev *et al.*[37] was added on Ni 3d and Co 3d electrons, where U = 6.6, 4.4, and 6.7 eV for Ni(Oh), Co(Td), and Co(Oh), respectively. The choice of U values is based on the work conducted by Shi *et al.*;[30] those values were determined on the basis of linear response theory and have been proved to successfully explain the magnetic and spin properties of spinel $NiCo_2O_4$, leading to adequate reproduction of experimentally measured magnetic moments of those cations.[38] As nickel at tetrahedral sites was not investigated in Shi's work,[30] we postulated a U value for Ni(Td) according to the equation:

$$U(\mathrm{Ni(Td)}) = \frac{U(Co(\mathrm{Td}))U(\mathrm{Ni(Oh)})}{U(Co(\mathrm{Oh}))} \quad (3)$$

This equation yields a value of 4.3 eV. To better understand the effect of the U term in our system, we have carried out calculations in primitive cells with selected U values from previous works.[27,39] The magnetic moments, charges, and electronic structures might vary due to different U values on Ni and Co ions. Thus, all U values equal to 3 eV were also tested to verify the overall trend and correlations of desired properties.

We have studied both $NiCo_2O_4$ primitive and conventional unit cells in this work. The primitive unit cell is composed of 14 atoms, $Ni_2Co_4O_8$, which contains two formula units (f.u.). The number of possible cation arrangements in a primitive unit cell is 6!/(4!2!) = 15, whereas there are only 3 symmetrically inequivalent configurations, i.e., inverse (DOI = 1, space group: *Imma*), 50% intermediate (DOI = 0.5, space group: *R*3*m*), and normal (DOI = 0, space group: *Fd*3*m*).[40] In addition to the simplicity, the use of a primitive cell has been proved to sufficiently explain the properties of spinel oxide observed in experiments.[41,42] The conventional unit cell with 56 atoms allows the investigation of 9 different DOIs, which were further studied to understand more the influence of the cation distribution. For the integration of a Brillouin zone, a 3 × 3 × 3 Monkhorst-Pack[43] k-point mesh was used for both primitive and conventional unit cells. A finer k-point mesh of 14 × 14 × 14 was used for the primitive unit cell to better sample the reciprocal space for the density of state (DOS) calculations. The self-consistent calculation was converged in 10^{-5} eV, and structural optimization was executed by minimizing forces on all the atoms until they were smaller than 0.01 eV $Å^{-1}$. Atomic charges were discussed using Bader charge analysis,[44] where the code from Henkelman *et al.* was applied.[45,46]

3. RESULTS AND DISCUSSION

3.1. Equilibrium Structures. We first investigated the stability and geometry of the different $NiCo_2O_4$ equilibrium structures in different degrees of inversion (DOI). Table 1 shows the computed lattice constants for both conventional and primitive unit cells and calculated relative and doping energies for corresponding DOIs.

Table 1. Calculated Lattice Constants, Relative Energies, and Doping Energies of $(Co_xNi_{1-x})_{Td}(Co_{2-x}Ni_x)_{Oh}O_4$ for Different DOIs

	lattice constant (Å)			
DOI (x)	conventional unit cell	primitive unit cell	relative energy (eV/f.u.)	doping energy (eV/f.u.)
1	8.178	8.16	0	−0.40
0.875	8.175		0.14	−0.26
0.75	8.160		0.28	−0.12
0.625	8.150		0.41	0.01
0.5	8.138	8.12	0.56	0.16
0.375	8.125		0.65	0.25
0.25	8.110		0.74	0.33
0.125	8.100		0.83	0.43
0	8.085	8.08	1.70	1.30

For the conventional unit cell, the computed lattice constant of inverse $NiCo_2O_4$ is 8.178 Å, which is merely 0.7% larger than the experimentally measured lattice constant 8.115 Å[47] and 0.7% smaller than the previous computational lattice constant 8.237 Å,[30] suggesting that a reliable computational setting has been used. It is clear that for both primitive and conventional cells, the lattice constant decreases continuously as $NiCo_2O_4$ transforms from an inverse to normal config-

https://doi.org/10.1021/acsomega.1c00295
ACS Omega XXXX, XXX, XXX−XXX

uration, consistent with the previous report that lattice parameters of the spinel are dependent on DOI.[31] It is expectable to acquire slightly different lattice constants for the conventional and primitive unit cells for the same DOI after structural optimization within periodic boundary conditions. The relative energy of the structure rises steadily from 0 to 1.7 eV as DOI decreases from 1 to 0, which indicates that the inverse structure is the most thermodynamically stable, in good agreement with the experimental results seen in the literature.[48−51]

Because $NiCo_2O_4$ can be regarded as Ni-doped Co_3O_4, their geometry stability can be described by the doping energy, expressed as follows:[30]

$$E_{\text{doping}(x)} = E_{(Co_xNi_{1-x})_{Td}(Co_{2-x}Ni_x)_{Oh}O_4} - E_{Co_3O_4} - E_{NiO} + E_{CoO} \quad (4)$$

where $E_{NiCo_2O_4}$ is the total energy of the $NiCo_2O_4$ in the corresponding DOI (x = 0 to 1); $E_{Co_3O_4}$, E_{NiO}, and E_{CoO} are the total energies of Co_3O_4 bulk, NiO bulk, and CoO bulk, respectively.

The calculated doping energy represents the stability of the $NiCo_2O_4$ structure compared to the parent compounds (i.e., Co_3O_4, NiO, and CoO bulks), indicating whether the formation of the structure in a certain degree of inversion is favorable or not. The high-DOI $NiCo_2O_4$ (x = 0.75 to 1) exhibits negative doping energies (under −0.12 eV/f.u.), suggesting that its formation is slightly thermodynamically favorable, whereas the structures with low DOI (x = 0 to 0.625) exhibit small positive doping energies, suggesting the formation of these DOIs are thermodynamically unfavorable. These results suggest that all $NiCo_2O_4$ in a higher DOI can be synthesised easily. Although the low-DOI $NiCo_2O_4$ seems unstable, its synthesis should still be possible under certain synthetic conditions, by taking into account the entropic effects caused by temperature.[51]

3.2. Crystal Field Stabilization Effects. For transition metal oxides with the spinel structure, crystal field theory (CFT) has been applied to predict the cation distribution and magnetic moments.[52−54] Chemical bonding has been treated as purely ionic, where each oxygen anion should be regarded as a point charge of −2. In spinel oxides, oxygen is arranged in a face-centered cubic structure, which forms tetrahedral holes and octahedral holes between oxygen atoms. The transition metal cations, which can randomly occupy both tetrahedral sites and octahedral sites, possess split d orbitals due to the electric field caused by oxygen anions. At octahedral sites, the d orbitals of each cation split into two energy levels, e_g and t_{2g}. On the other hand, at tetrahedral sites, the d orbitals split into e and t_2 levels. As a result, d electrons prefer to occupy the split orbitals in the configuration, where the overall energy is the lowest. The final cation distribution is only dependent on the crystal field stabilization energy, which does not take any other effects such as cation size and covalent bonding into account. It is well known that CFT is oversimplified because of those assumptions; however, the crystal field stabilization effect is still an important factor, which affects how the cations are arranged in the spinel structure. Therefore, in this section, the crystal field stabilization energy (CFSE) and octahedral site preference energy (OSPE) derived from CFT are provided to investigate potential correlations with our DFT results. CFT predicts that the oxygen anion with a face-centered cubic structure is a relatively weak ligand and induces slight d orbital splitting.[55,56] In this case, cations that reside in tetrahedral sites have high-spin electron occupation; in comparison, those occupying octahedral sites may either have high-spin or low-spin configurations.[57] In order to describe qualitatively the crystal field stabilization effects, CFSE and OSPE for Ni^{2+}, Ni^{3+}, Co^{2+}, and Co^{3+} are listed in Table S1.

3.3. Atomic Charges and Magnetic Moments. Understanding how DOI influences the oxidation state is the major motivation of this work. By using Bader charge analysis, a series of $NiCo_2O_4$ spinel oxides with various DOIs were computed to investigate the relationship between the oxidation state and cation distribution. The obtained charges and magnetic moments of Ni and Co cations in primitive cells are listed in Table 2. In the literature, Ni and Co have been reported to possess various oxidation states, ranging from +2 to +3.[58−60] This phenomenon may result from the complex cation distribution in spinel oxides because the cation, which has a certain oxidation state, can be stabilized more in a specific position, as predicted by CFT.[40] In this section, three structures (inverse, 50% intermediate, and normal) in primitive cells are considered preliminarily, in order to assess the variation of oxidation states and magnetic moments in different cation arrangements. Note that all calculated cation charges are underestimated compared to their formal oxidation state, which is common for the GGA functional and Bader analysis.[61−63] In the fully inverse spinel, the charge of octahedrally coordinated Ni(Oh) is +1.20 |e|, while Co(Td) and Co(Oh) possess charges of +1.49 and +1.38 |e|, respectively. On the other hand, Ni occupies tetrahedral sites in the normal spinel, with all Co cations in octahedral positions. In such configuration, Ni is calculated to be +1.21 |e|, whereas Co has a charge of +1.32 |e|. By making the assumption that the Bader charge of the atom is correlated to the atom's oxidation state, it is expected that the valence electrons of cations may experience a significant change while being swapped to different positions. Comparing the 50% intermediate structure to the inverse and normal structures, Ni(Td) exhibits a higher oxidation state compared with the normal spinel (+1.33 versus +1.21 |e|), whereas Co(Td) shows

Table 2. Bader Charges (Q, in |e|), Assigned Formal Charges, and the Numbers of Projected Unpaired Electron ($N_\alpha - N_\beta$) of Ni and Co at Tetrahedral and Octahedral Sites and the Total Magnetization per Formula Unit ($N_\alpha - N_{\beta,\text{ total}}$) of the Inverse, 50% Intermediate, and Normal $NiCo_2O_4$ in a Primitive Unit Cell

cations	properties	inverse	50% intermediate	normal
Ni(Td)	Q		+1.33	+1.21
	formal charge		+2 to +3	∼+2
	$N_\alpha - N_\beta$		1.998	1.791
Ni(Oh)	Q	+1.20	+1.19	
	formal charge	∼+2	∼+2	
	$N_\alpha - N_\beta$	−1.670	−1.661	
Co(Td)	Q	+1.49	+1.33	
	formal charge	∼+3	+2 to +3	
	$N_\alpha - N_\beta$	3.022	2.696	
Co(Oh)	Q	+1.38	+1.35	+1.32
	formal charge	+3	+3	+3
	$N_\alpha - N_\beta$	0.060	0.070	−0.260
	$N_\alpha - N_{\beta,\text{ total}}$	2	2	2

https://doi.org/10.1021/acsomega.1c00295
ACS Omega XXXX, XXX, XXX−XXX

an obvious decrease in the oxidation state compared to the inverse structure (+1.33 versus +1.49 |e|). All minor changes in charges, which occur in Ni(Oh) and Co(Oh), may be ascribed to the balance of total charge in order to maintain the charge neutrality. In order to compare the effects of different U values, a set of U values (3 eV for all cations, reported by Stevanović *et al.*[39]) are computed as well, and the Bader charge analysis and magnetic moments are shown in Table S2. The trend observed is similar for all DOIs, with slightly different charges and magnetic moments.

The Bader charge results exhibit a relationship between the oxidation state of cations and DOI. However, a further explanation of the Bader analysis is required to correlate the obtained Bader charge with the formal charge of cations in real $NiCo_2O_4$. Although the magnetic moment is not typically reported to affect the catalytic activities of $NiCo_2O_4$, it can help to understand the occupation of d orbitals of Ni and Co, and thus the formal charge of each cation. When considering the magnetic moments along with the charges obtained in the DFT calculations, formal charges (Table 2) and electronic configurations (in Figure 2a–c) of $NiCo_2O_4$ at corresponding

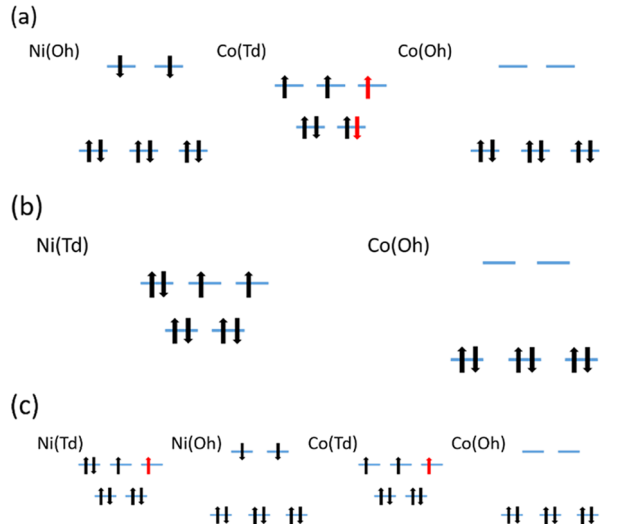

Figure 2. Proposed electronic configurations of the 3d orbitals of Ni and Co ions at octahedral and tetrahedral sites of (a) inverse, (b) normal, and (c) 50% intermediate structures. Black arrows indicate full occupation of electrons, and red arrows represent partial occupation.

DOIs (inverse, normal, and 50% intermediate) can be estimated. Two important assumptions should be made prior to the assignment of formal charges. First, the Bader charges can only be compared between the same atoms at the same sites in various DOIs; i.e., Co(Td) with a charge of +1.49 is not necessary to be more positive than Co(Oh) of +1.38. The comparison between two Bader charges is only made when the cations are in similar environments (i.e., tetrahedral or octahedral sites). Second, the formal charges are rounded to an integer, due to known underestimates by GGA and Bader analysis; i.e., all charges are rounded up based on comparisons between the calculated results and known experimental results, making the assumption that there is a correlation between the calculated Bader charge and formal oxidation charge on the atom. Note that some formal charges with a tilde mark means that they are close to an integer (e.g., ∼+3 represents that the charge is close to +3), which is reasonable owing to the partial occupation of d orbitals.[30] The assignment of the electronic configuration starts from the fact that Co(Oh) has been commonly reported to possess a charge of +3 and is nonmagnetic,[30,64,65] which is also confirmed by our calculated magnetic moment (see Table 2). In the inverse structure, Co(Td) is assigned a formal charge near +3 by referring to the obtained magnetic moment. The formal charge of Ni(Oh) is assigned to be close to +2, considering the calculated magnetic moment ($-1.67\ \mu_B$) and the overall formal charge is close to +8. Figure 2a shows the predicted electron occupation in d orbitals for the inverse $NiCo_2O_4$ based on the oxidation states and magnetic moments in Table 2. Regarding the normal spinel structure, the Ni(Td) should be near +2 to fulfil the overall +8 formal charge because each Co(Oh) possesses a +3 charge. The proposed electronic configuration of the normal spinel based on Table 2 is shown in Figure 2b. As a more complex system, 50% intermediate $NiCo_2O_4$ is of great interest and worth researching. In 50% intermediate $NiCo_2O_4$, Co(Oh) remains +3 in this structure, while Co(Td) has been assigned a formal charge between +2 and +3 according to the Bader charge and magnetic moment, which is also in line with the literature reporting that Co(Td) can be a mix of +2 and +3 cations.[24,26,60] Ni(Oh) displays a similar Bader charge to the one in inverse $NiCo_2O_4$, so the proposed oxidation state for Ni(Oh) is +2 as well. However, Ni(Td) exhibits a more positive Bader charge compared to that of normal $NiCo_2O_4$, resulting in a higher formal charge than that of the normal $NiCo_2O_4$. Therefore, Ni(Td) in the 50% intermediate is assigned to range from +2 to +3.

To further probe the relationship between the oxidation state and DOI, more DOIs were taken into account in conventional cells, and the results are shown in Figure 3. All

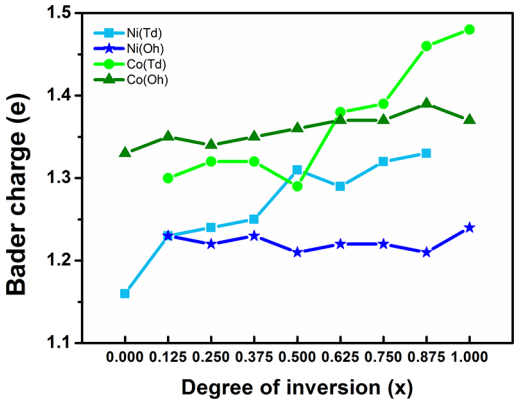

Figure 3. Average Bader charges of all the Ni and Co atoms at both tetrahedral and octahedral sites in a $NiCo_2O_4$ conventional unit cell.

cations maintain almost an unchanged oxidation state at octahedral sites regardless of whether the sites are occupied by Ni or Co. By contrast, both Ni(Td) and Co(Td) generally experience an increase in the charge. This result indicates that Ni(Td) and Co(Td) are cations that are more likely to be altered/optimized in the synthesis of $NiCo_2O_4$ because they experience large changes in oxidation states as DOI changes. Note that when the DOI is 0.5, there is a deviation from the general trend of increasing oxidation states for Co(Td) and Ni(Td). The reason remains unclear at the current stage and may need future investigations. Despite the deviation observed for 50% intermediate spinel, a general relationship between the oxidation state and DOI is clearly illustrated.

https://doi.org/10.1021/acsomega.1c00295
ACS Omega XXXX, XXX, XXX−XXX

The CFT predictions and experimental results in the literature are compared carefully with our DFT results. First, the CFT and OSPE expect that Ni^{2+} prefers octahedral sites, which matches our calculations and experimental results in the literature (see Table 2 and Table S1).[24,66−71] For Ni^{3+} cations, CFT also predicts that Ni^{3+} with a low-spin state favors the occupation of octahedral sites (see Table S1), which is not in agreement with our calculations. Nevertheless, it is common to observe tetrahedrally coordinated Ni^{3+} in synthesized $NiCo_2O_4$ spinel,[22,58,66] which is consistent with our results. This discrepancy between CFT and experimental results may be ascribed to the oversimplified crystal field theory. Ni^{3+} with a high-spin state, which has a less negative OSPE value, is theoretically more likely to stay in tetrahedral sites. On the other hand, CFT expects that Co^{3+} with a low-spin state substantially tends to reside in octahedral sites, which agrees with the results from our calculations and in the literature.[66,69] Therefore, a high-spin Co^{3+} cation is less possible to exist in octahedral positions.[71] Though the Co^{2+} is predicted by CFT to prefer octahedral sites as well, the affinity is not as strong as Co^{3+}. Therefore, Co^{2+} is observed mainly in tetrahedral holes. The assignment of Co^{2+} and Co^{3+} is in good consistency with $NiCo_2O_4$ synthesized by different methods, studied by Marco *et al.* and Kim *et al.*[59,71] Although CFT is a simple model that only considers the electrostatic forces between cations and anions, surprisingly, it performs well in predicting the cation distribution in the case of $NiCo_2O_4$, which validates the application of the OSPE model to simply and quickly explain the different cation arrangements and electronic structures of $NiCo_2O_4$ in the literature.

3.4. Density of States. Density of state (DOS) calculations were used to analyze how DOI of $NiCo_2O_4$ affects its corresponding electronic structure. The projected DOS in Figure 4a shows that the inverse $NiCo_2O_4$ has a band gap of 0.9 eV, consistent with the previous study, which used similar U terms.[72] Also, an integer magnetic moment of the entire system was set as 2 μ_B per formula unit based on the previous work.[73,74] If there is a band gap in at least one spin channel, the number of electrons in that channel(s) should be an integer. The number of electrons with the opposite spin is also an integer, so the total magnetization per formula unit is an integer as well. The integer magnetic moment criterion can be used to distinguish half metals and insulators from metals.[75] This methodology is applied here because $NiCo_2O_4$ is a semiconductor.

In the inverse structure, the main contribution to the states around the Fermi level is strongly hybridized O 2p, Ni(Oh), and Co(Td) 3d orbitals in the minority spin, shown in Figure 4a. Moreover, at all energy levels in both spin channels, hybridization is significant between cation 3d and O 2p orbitals, which may lead to different crystal field splitting effects of cation 3d orbitals and thus influence the electron occupancy. For example, the occupancies of Co(Oh) in the inverse structure in Table S3 show that Co(Oh) has 71 and 72% occupancies for the spin up and spin down, respectively. The occupancies estimated by DOS are not exactly the same as our proposed electronic structure (60% for both spin up and spin down, see Figure 2a) based on our assigned formal charge +3 in Table 2, which may be owing to the hybridization of d and p orbitals. Despite the small difference in the electron occupancy, the DOS results still suggest that Co(Oh) is nonmagnetic, supporting our assumption in Section 3.3 again. Generally speaking, the d orbital occupancy obtained from the

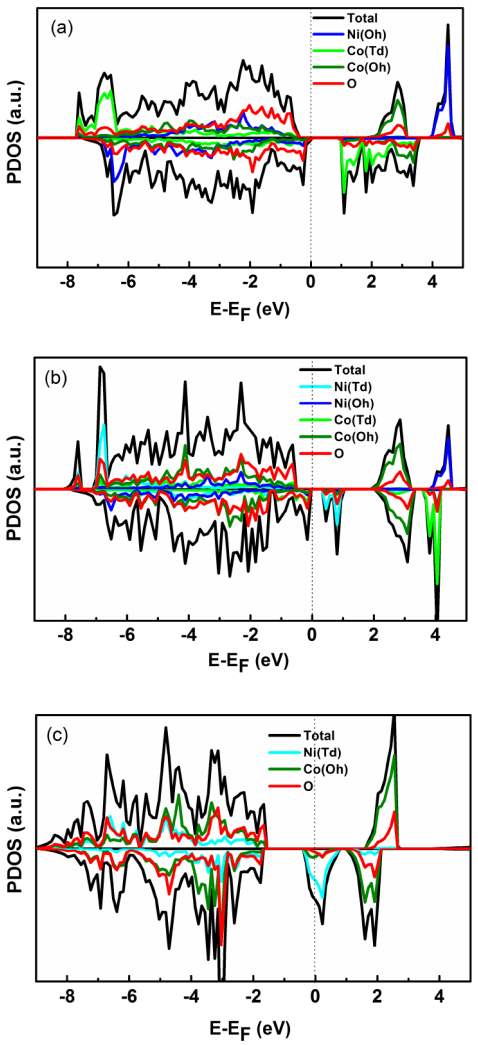

Figure 4. Projected density of state (PDOS) of (a) inverse (b) 50% intermediate, and (c) normal $NiCo_2O_4$.

DOS fits well with our proposed electronic configurations in the previous section, which confirms that our assignments for oxidation states of cations are reasonable.

For the 50% intermediate structure (see Figure 4b), $NiCo_2O_4$ has a smaller band gap of 0.36 eV and is insulating, which follows again its integer criterion of magnetic moment (Table 2). This band gap is quite close to what Ndione *et al.* reported (approximately 0.3 eV).[27] In this cation configuration, O 2p is still highly hybridized with cation 3d orbitals in both valence and conduction bands. Again, the d orbital occupancy acquired from the DOS results is given in Table S4, which is very close to our prediction of electronic configurations. The difference between Bader charge analysis and DOS may be attributed to the partially localized d orbitals and the hybridization effects. Note that there is tiny magnetization for Co(Oh) from DOS calculation (74 and 69% occupancy for up and down spins, respectively); however, this magnetic moment is negligible when the electronic configuration is assigned in the previous section, suggesting that we can follow the assumption of zero magnetization for Co(Oh), based on the literature data.

For the normal spinel structure (see Figure 4c), half-metallicity, which is contributed by O 2p, Co(Oh), and Ni(Td) orbitals, is shown in our DOS calculation with an

https://doi.org/10.1021/acsomega.1c00295
ACS Omega XXXX, XXX, XXX−XXX

integer magnetic moment (Table 2), which obeys the integer magnetic moment criterion. The resultant DOS resembles the result using similar *U* terms completed by Pandey *et al.*, which exhibits great consistency, compared to our calculations.[72] O 2p is also strongly hybridized with Co(Oh) and Ni(Td) for all energy levels. The d orbital occupancy integrated from the DOS results is provided in Table S5, which is close to our prediction of electronic configurations, apart from the little discrepancy between the Co(Oh) occupancy of DOS (Table S5) and proposed electronic configuration (Figure 2b). Note that the discrepancy between our proposed electronic configurations and the orbital occupancy is expected to occur because we apply the nonmagnetic Co(Oh) assumption for all spinel structures when assigning the occupancy.

Overall, the projected DOS results (Figure 4a−c) demonstrate that our proposed electronic configurations for the inverse, 50% intermediate, and normal $NiCo_2O_4$ are valid and exhibit a good agreement with the DOS presented in the literature. In all DOS calculations, hybridization of O 2p and metal cation 3d orbitals is observed, implying the possible covalent effect on the cation distribution and electronic structure, but the crystal field splitting effect is still the dominant factor for the $NiCo_2O_4$, confirmed by our calculation and OSPE model.

4. CONCLUSIONS

We investigated the equilibrium structures and relative stabilities of $NiCo_2O_4$ with various degrees of inversion (DOIs). The high-DOI $NiCo_2O_4$ is computed to be energetically favorable, and low-DOI ones have tiny positive doping energies, suggesting that it is still possible to produce lower DOI $NiCo_2O_4$ via some synthesis routes. In our DFT calculations, Ni(Td) and Co(Td) are found to undergo significant changes in the oxidation state, suggesting that the desired oxidation state may be modulated by altering the DOI. In comparison, Ni(Oh) and Co(Oh) remain almost unchanged as the DOI changes. The crystal field theory and the consequent crystal field stabilization energy are also compared in this work, supporting the trends we found for the cation distribution in all $NiCo_2O_4$ crystal models. The DOS results also confirm that the predicted d-band occupancy agrees with the formal charges assigned to the Ni and Co cations.

In summary, by combining the Bader charge analysis and magnetic moments of cations, the formal charges and electronic structures of $NiCo_2O_4$ can be evaluated systematically, and the results are in good agreement with the widely used crystal field theory. The confirmation of Ni/Co oxidation states via different analyses could be essential for further understanding of electrochemical/catalytic performance.

■ ASSOCIATED CONTENT

Supporting Information

The Supporting Information is available free of charge at https://pubs.acs.org/doi/10.1021/acsomega.1c00295.

Crystal field stabilization energy (CFSE) and octahedral site preference energy (OSPE) for Ni^{2+}, Ni^{3+}, Co^{2+}, and Co^{3+} cations (Table S1); Bader charges, assigned formal charges, and numbers of projected unpaired electron of Ni and Co at tetrahedral and octahedral sites, calculated with all *U* terms being 3 eV (Table S2); electronic occupancy of inverse $NiCo_2O_4$ obtained from the density of state (Table S3); electronic occupancy of 50% intermediate $NiCo_2O_4$ obtained from the density of state (Table S4); and electronic occupancy of normal $NiCo_2O_4$ obtained from the density of state (Table S5) (PDF)

■ AUTHOR INFORMATION

Corresponding Author

Hsin-Yi Tiffany Chen − *Department of Engineering and System Science, National Tsing Hua University, Hsinchu 300044, Taiwan;* orcid.org/0000-0002-9651-3200; Email: hsinyi.tiffany.chen@gapp.nthu.edu.tw

Authors

Tzu-Chien Chang − *Department of Engineering and System Science, National Tsing Hua University, Hsinchu 300044, Taiwan*

Yi-Ting Lu − *Department of Chemical Engineering, National Tsing Hua University, Hsinchu 300044, Taiwan; Stephenson Institute for Renewable Energy, Department of Chemistry, University of Liverpool, Liverpool L69 7ZF, U.K.;* orcid.org/0000-0003-2128-1385

Chih-Heng Lee − *Department of Engineering and System Science, National Tsing Hua University, Hsinchu 300044, Taiwan*

Jyoti K. Gupta − *Stephenson Institute for Renewable Energy, Department of Chemistry, University of Liverpool, Liverpool L69 7ZF, U.K.*

Laurence J. Hardwick − *Stephenson Institute for Renewable Energy, Department of Chemistry, University of Liverpool, Liverpool L69 7ZF, U.K.;* orcid.org/0000-0001-8796-685X

Chi-Chang Hu − *Department of Chemical Engineering, National Tsing Hua University, Hsinchu 300044, Taiwan;* orcid.org/0000-0002-4308-8474

Complete contact information is available at: https://pubs.acs.org/10.1021/acsomega.1c00295

Author Contributions

#T.-C.C. and Y.-T.L. contributed equally to this work.

Notes

The authors declare no competing financial interest.

■ ACKNOWLEDGMENTS

T.-C.C., Y.-T.L., C.-H.L., and H.-Y.T.C. acknowledge financial support provided by the Ministry of Science and Technology (MOST) (108-2112-M-007-023-MY3 and 109-3116-F-007-001), the National Tsing Hua University grants (109Q2716E1 and 109Q2708E1), and the computing resource of TAIWANIA in the National Center for High-Performance Computing (NCHC) in Taiwan. Y.-T.L. and C.-C.H. acknowledge funding from MOST 108-2221-E-007-072-MY3. J.K.G. and L.J.H. acknowledge funding from the Engineering and Physical Sciences Research Council (EPSRC) grants EP/R020744/1 and EP/R000441/1. L.J.H., C.-C.H., and Y.-T.L. acknowledge the cooperative framework set up between the National Tsing Hua University, Taiwan and University of Liverpool, UK.

■ REFERENCES

(1) Ma, C.; Xu, N.; Qiao, J.; Jian, S.; Zhang, J. Facile synthesis of $NiCo_2O_4$ nanosphere-carbon nanotubes hybrid as an efficient

bifunctional electrocatalyst for rechargeable Zn−air batteries. *Int. J. Hydrogen Energy* **2016**, *41*, 9211−9218.
(2) Liu, L.; Wang, J.; Hou, Y.; Chen, J.; Liu, H.-K.; Wang, J.; Wu, Y. Self-Assembled 3D Foam-Like $NiCo_2O_4$ as Efficient Catalyst for Lithium Oxygen Batteries. *Small* **2016**, *12*, 602−611.
(3) Li, L.; Shen, L.; Nie, P.; Pang, G.; Wang, J.; Li, H.; Dong, S.; Zhang, X. Porous $NiCo_2O_4$ nanotubes as a noble-metal-free effective bifunctional catalyst for rechargeable Li−O_2 batteries. *J. Mater. Chem. A* **2015**, *3*, 24309−24314.
(4) Lee, D. U.; Park, M. G.; Cano, Z. P.; Ahn, W.; Chen, Z. Hierarchical Core−Shell Nickel Cobaltite Chestnut-like Structures as Bifunctional Electrocatalyst for Rechargeable Metal−Air Batteries. *ChemSusChem* **2018**, *11*, 406−414.
(5) Prabu, M.; Ketpang, K.; Shanmugam, S. Hierarchical nanostructured $NiCo_2O_4$ as an efficient bifunctional non-precious metal catalyst for rechargeable zinc−air batteries. *Nanoscale* **2014**, *6*, 3173−3181.
(6) Zheng, Y.; Lin, Z.; Chen, W.; Liang, B.; Du, H.; Yang, R.; He, X.; Tang, Z.; Gui, X. Flexible, sandwich-like CNTs/$NiCo_2O_4$ hybrid paper electrodes for all-solid state supercapacitors. *J. Mater. Chem. A* **2017**, *5*, 5886−5894.
(7) Guo, D.; Zhang, L.; Song, X.; Tan, L.; Ma, H.; Jiao, J.; Zhu, D.; Li, F. $NiCo_2O_4$ nanosheets grown on interconnected honeycomb-like porous biomass carbon for high performance asymmetric supercapacitors. *New J. Chem.* **2018**, *42*, 8478−8484.
(8) Bhagwan, J.; Nagaraju, G.; Ramulu, B.; Sekhar, S. C.; Yu, J. S. Rapid synthesis of hexagonal $NiCo_2O_4$ nanostructures for high-performance asymmetric supercapacitors. *Electrochim. Acta* **2019**, *299*, 509−517.
(9) Wang, Q.; Bai, J.; Huang, B.; Hu, Q.; Cheng, X.; Li, J.; Xie, E.; Wang, Y.; Pan, X. Design of $NiCo_2O_4$@SnO_2 heterostructure nanofiber and their low temperature ethanol sensing properties. *J. Alloys Compd.* **2019**, *791*, 1025−1032.
(10) Huang, W.; Cao, Y.; Chen, Y.; Peng, J.; Lai, X.; Tu, J. Fast synthesis of porous $NiCo_2O_4$ hollow nanospheres for a high-sensitivity non-enzymatic glucose sensor. *Appl. Surf. Sci.* **2017**, *396*, 804−811.
(11) Xue, B.; Li, K.; Feng, L.; Lu, J.; Zhang, L. Graphene wrapped porous Co_3O_4/$NiCo_2O_4$ double-shelled nanocages with enhanced electrocatalytic performance for glucose sensor. *Electrochim. Acta* **2017**, *239*, 36−44.
(12) Fang, L.; Jiang, Z.; Xu, H.; Liu, L.; Guan, Y.; Gu, X.; Wang, Y. Crystal-plane engineering of $NiCo_2O_4$ electrocatalysts towards efficient overall water splitting. *J. Catal.* **2018**, *357*, 238−246.
(13) Gao, X.; Zhang, H.; Li, Q.; Yu, X.; Hong, Z.; Zhang, X.; Liang, C.; Lin, Z. Hierarchical $NiCo_2O_4$ Hollow Microcuboids as Bifunctional Electrocatalysts for Overall Water-Splitting. *Angew. Chem., Int. Ed.* **2016**, *55*, 6290−6294.
(14) Chen, S.; Qiao, S.-Z. Hierarchically Porous Nitrogen-Doped Graphene−$NiCo_2O_4$ Hybrid Paper as an Advanced Electrocatalytic Water-Splitting Material. *ACS Nano* **2013**, *7*, 10190−10196.
(15) Wang, Z.; Jiang, M.; Qin, J.; Zhou, H.; Ding, Z. Reinforced photocatalytic reduction of CO_2 to CO by a ternary metal oxide $NiCo_2O_4$. *Phys. Chem. Chem. Phys.* **2015**, *17*, 16040−16046.
(16) Liu, J.; Zhang, J.; Wang, D.; Li, D.; Ke, J.; Wang, S.; Liu, S.; Xiao, H.; Wang, R. Highly Dispersed $NiCo_2O_4$ Nanodots Decorated Three-Dimensional g-C_3N_4 for Enhanced Photocatalytic H_2 Generation. *ACS Sustainable Chem. Eng.* **2019**, *7*, 12428−12438.
(17) Jiang, J.; Shi, W.; Guo, F.; Yuan, S. Preparation of magnetically separable and recyclable carbon dots/$NiCo_2O_4$ composites with enhanced photocatalytic activity for the degradation of tetracycline under visible light. *Inorg. Chem. Front.* **2018**, *5*, 1438−1444.
(18) Huang, Y.; Fan, W.; Long, B.; Li, H.; Qiu, W.; Zhao, F.; Tong, Y.; Ji, H. Alkali-modified non-precious metal 3D-$NiCo_2O_4$ nanosheets for efficient formaldehyde oxidation at low temperature. *J. Mater. Chem. A* **2016**, *4*, 3648−3654.
(19) Xiao, J.; Kuang, Q.; Yang, S.; Xiao, F.; Wang, S.; Guo, L. Surface structure dependent electrocatalytic activity of Co_3O_4 anchored on graphene sheets toward oxygen reduction reaction. *Sci. Rep.* **2013**, *3*, 2300.
(20) Zhao, J.; He, Y.; Chen, Z.; Zheng, X.; Han, X.; Rao, D.; Zhong, C.; Hu, W.; Deng, Y. Engineering the Surface Metal Active Sites of Nickel Cobalt Oxide Nanoplates toward Enhanced Oxygen Electrocatalysis for Zn−Air Battery. *ACS Appl. Mater. Interfaces* **2019**, 4915−4921.
(21) Yang, L.; Zhang, B.; Fang, B.; Feng, L. A comparative study of $NiCo_2O_4$ catalyst supported on Ni foam and from solution residuals fabricated by a hydrothermal approach for electrochemical oxygen evolution reaction. *Chem. Commun.* **2018**, *54*, 13151−13154.
(22) Wang, H.-Y.; Hsu, Y.-Y.; Chen, R.; Chan, T.-S.; Chen, H. M.; Liu, B. Ni^{3+} Induced Formation of Active NiOOH on the Spinel Ni−Co Oxide Surface for Efficient Oxygen Evolution Reaction. *Adv. Energy Mater.* **2015**, *5*, 1500091.
(23) Lu, Y.-T.; Chien, Y.-J.; Liu, C.-F.; You, T.-H.; Hu, C.-C. Active site-engineered bifunctional electrocatalysts of ternary spinel oxides, $M_{0.1}Ni_{0.9}Co_2O_4$ (M: Mn, Fe, Cu, Zn) for the air electrode of rechargeable zinc−air batteries. *J. Mater. Chem. A* **2017**, *5*, 21016−21026.
(24) Lenglet, M.; Guillamet, R.; Dürr, J.; Gryffroy, D.; Vandenberghe, R. E. Electronic structure of $NiCo_2O_4$ by XANES, EXAFS and ^{61}Ni Mössbauer studies. *Solid State Commun.* **1990**, *74*, 1035−1039.
(25) Stevanović, V.; d'Avezac, M.; Zunger, A. Universal electrostatic origin of cation ordering in A_2BO_4 spinel oxides. *J. Am. Chem. Soc.* **2011**, *133*, 11649−11654.
(26) Iliev, M. N.; Silwal, P.; Loukya, B.; Datta, R.; Kim, D. H.; Todorov, N. D.; Pachauri, N.; Gupta, A. Raman studies of cation distribution and thermal stability of epitaxial spinel $NiCo_2O_4$ films. *J. Appl. Phys.* **2013**, *114*, No. 033514.
(27) Ndione, P. F.; Shi, Y.; Stevanovic, V.; Lany, S.; Zakutayev, A.; Parilla, P. A.; Perkins, J. D.; Berry, J. J.; Ginley, D. S.; Toney, M. F. Control of the electrical properties in spinel oxides by manipulating the cation disorder. *Adv. Funct. Mater.* **2014**, *24*, 610−618.
(28) Liu, Y.; Liu, P.; Qin, W.; Wu, X.; Yang, G. Laser modification-induced $NiCo_2O_{4-\delta}$ with high exterior Ni^{3+}/Ni^{2+} ratio and substantial oxygen vacancies for electrocatalysis. *Electrochim. Acta* **2019**, *297*, 623−632.
(29) Shi, X.; Bernasek, S. L.; Selloni, A. Oxygen deficiency and reactivity of spinel $NiCo_2O_4$ (001) surfaces. *J. Phys. Chem. C* **2017**, *121*, 3929−3937.
(30) Shi, X.; Bernasek, S. L.; Selloni, A. Formation, electronic structure, and defects of Ni substituted spinel cobalt oxide: a DFT + U study. *J. Phys. Chem. C* **2016**, *120*, 14892−14898.
(31) Fritsch, D.; Ederer, C. Effect of epitaxial strain on the cation distribution in spinel ferrites $CoFe_2O_4$ and $NiFe_2O_4$: A density functional theory study. *Appl. Phys. Lett.* **2011**, *99*, No. 081916.
(32) Dileep, K.; Loukya, B.; Silwal, P.; Gupta, A.; Datta, R. Probing optical band gaps at nanoscale from tetrahedral cation vacancy defects and variation of cation ordering in $NiCo_2O_4$ epitaxial thin films. *J. Phys. D: Appl. Phys.* **2014**, *47*, 405001.
(33) Kresse, G.; Joubert, D. From ultrasoft pseudopotentials to the projector augmented-wave method. *Phys. Rev. B* **1999**, *59*, 1758.
(34) Hafner, J. Ab-initio simulations of materials using VASP: Density-functional theory and beyond. *J. Comput. Chem.* **2008**, *29*, 2044−2078.
(35) Perdew, J. P.; Burke, K.; Ernzerhof, M. Generalized gradient approximation made simple. *Phys. Rev. Lett.* **1996**, *77*, 3865.
(36) Perdew, J. P.; Yue, W. Accurate and simple density functional for the electronic exchange energy: Generalized gradient approximation. *Phys. Rev. B* **1986**, *33*, 8800.
(37) Dudarev, S. L.; Botton, G. A.; Savrasov, S. Y.; Humphreys, C. J.; Sutton, A. P. Electron-energy-loss spectra and the structural stability of nickel oxide: An LSDA + U study. *Phys. Rev. B* **1998**, *57*, 1505.
(38) Cococcioni, M.; De Gironcoli, S. Linear response approach to the calculation of the effective interaction parameters in the LDA + U method. *Phys. Rev. B* **2005**, *71*, No. 035105.

https://doi.org/10.1021/acsomega.1c00295
ACS Omega XXXX, XXX, XXX−XXX

(39) Stevanović, V.; Lany, S.; Zhang, X.; Zunger, A. Correcting density functional theory for accurate predictions of compound enthalpies of formation: Fitted elemental-phase reference energies. *Phys. Rev. B* **2012**, *85*, 115104.
(40) Santos-Carballal, D.; Ngoepe, P. E.; de Leeuw, N. H. Ab initio investigation of the thermodynamics of cation distribution and of the electronic and magnetic structures in the $LiMn_2O_4$ spinel. *Phys. Rev. B* **2018**, *97*, No. 085126.
(41) Wei, S.-H.; Zhang, S. First-principles study of cation distribution in eighteen closed-shell $A^{II}B_2^{III}O_4$ and $A^{IV}B_2^{II}O_4$ spinel oxides. *Phys. Rev. B* **2001**, *63*, No. 045112.
(42) Walsh, A.; Wei, S.-H.; Yan, Y.; Al-Jassim, M. M.; Turner, J. A.; Woodhouse, M.; Parkinson, B. A. Structural, magnetic, and electronic properties of the Co-Fe-Al oxide spinel system: Density-functional theory calculations. *Phys. Rev. B* **2007**, *76*, 165119.
(43) Monkhorst, H. J.; Pack, J. D. Special points for Brillouin-zone integrations. *Phys. Rev. B* **1976**, *13*, 5188.
(44) Bader, R. F. W. A quantum theory of molecular structure and its applications. *Chem. Rev.* **1991**, *91*, 893−928.
(45) Tang, W.; Sanville, E.; Henkelman, G. A grid-based Bader analysis algorithm without lattice bias. *J. Phys.: Condens. Matter* **2009**, *21*, No. 084204.
(46) Sanville, E.; Kenny, S. D.; Smith, R.; Henkelman, G. Improved grid-based algorithm for Bader charge allocation. *J. Comput. Chem.* **2007**, *28*, 899−908.
(47) Nkeng, P.; Poillerat, G.; Koenig, J. F.; Chartier, P.; Lefez, B.; Lopitaux, J.; Lenglet, M. Characterization of Spinel-Type Cobalt and Nickel Oxide Thin Films by X-Ray Near Grazing Diffraction, Transmission and Reflectance Spectroscopies, and Cyclic Voltammetry. *J. Electrochem. Soc.* **1995**, *142*, 1777−1783.
(48) Knop, O.; Reid, K. I. G.; Sutarno; Nakagawa, Y. Chalkogenides of the transition elements. VI. X-Ray, neutron, and magnetic investigation of the spinels Co_3O_4, $NiCo_2O_4$, Co_3S_4, and $NiCo_2S_4$. *Can. J. Chem.* **1968**, *46*, 3463−3476.
(49) Anu Prathap, M. U.; Srivastava, R. Synthesis of $NiCo_2O_4$ and its application in the electrocatalytic oxidation of methanol. *Nano Energy* **2013**, *2*, 1046−1053.
(50) Shen, Y.; Kan, D.; Lin, I.-C.; Chu, M.-W.; Suzuki, I.; Shimakawa, Y. Perpendicular magnetic tunnel junctions based on half-metallic $NiCo_2O_4$. *Appl. Phys. Lett.* **2020**, *117*, No. 042408.
(51) Guo, W.; Zhen, C.; Wu, C.; Wu, X.; Li, G.; Ma, L.; Hou, D. Influence of growth temperature on the microstructure and electrical transport properties of epitaxial $NiCo_2O_4$ thin films. *Ceram. Int.* **2018**, *44*, 12539−12546.
(52) Burdett, J. K.; Price, G. D.; Price, S. L. Role of the crystal-field theory in determining the structures of spinels. *J. Am. Chem. Soc.* **1982**, *104*, 92−95.
(53) McClure, D. S. The distribution of transition metal cations in spinels. *J. Phys. Chem. Solids* **1957**, *3*, 311−317.
(54) Navrotsky, A.; Kleppa, O. J. The thermodynamics of cation distributions in simple spinels. *J. Inorg. Nucl. Chem.* **1967**, *29*, 2701−2714.
(55) Grosvenor, A. P.; Kobe, B. A.; Biesinger, M. C.; McIntyre, N. S. Investigation of multiplet splitting of Fe 2p XPS spectra and bonding in iron compounds. *Surf. Interface Anal.* **2004**, *36*, 1564−1574.
(56) Summerville, D. A.; Jones, R. D.; Hoffman, B. M.; Basolo, F. Chromium (III) porphyrins. Chemical and spectroscopic properties of chloro-meso-tetraphenylporphinatochromium (III) in nonaqueous solutions. *J. Am. Chem. Soc.* **1977**, *99*, 8195−8202.
(57) Dunitz, J. D.; Orgel, L. E. Electronic properties of transition-metal oxides-II: cation distribution amongst octahedral and tetrahedral sites. *J. Phys. Chem. Solids* **1957**, *3*, 318−323.
(58) Marco, J. F.; Gancedo, J. R.; Gracia, M.; Gautier, J. L.; Ríos, E. I.; Palmer, H. M.; Greaves, C.; Berry, F. J. Cation distribution and magnetic structure of the ferrimagnetic spinel $NiCo_2O_4$. *J. Mater. Chem.* **2001**, *11*, 3087−3093.
(59) Marco, J. F.; Gancedo, J. R.; Gracia, M.; Gautier, J. L.; Ríos, E.; Berry, F. J. Characterization of the nickel cobaltite, $NiCo_2O_4$, prepared by several methods: an XRD, XANES, EXAFS, and XPS study. *J. Solid State Chem.* **2000**, *153*, 74−81.
(60) Bitla, Y.; Chin, Y.-Y.; Lin, J.-C.; Van, C. N.; Liu, R.; Zhu, Y.; Liu, H.-J.; Zhan, Q.; Lin, H.-J.; Chen, C.-T.; Chu, Y.-H.; He, Q. Origin of metallic behavior in $NiCo_2O_4$ ferrimagnet. *Sci. Rep.* **2015**, *5*, 15201.
(61) Roldan, A.; Santos-Carballal, D.; de Leeuw, N. H. A comparative DFT study of the mechanical and electronic properties of greigite Fe_3S_4 and magnetite Fe_3O_4. *J. Chem. Phys.* **2013**, *138*, 204712.
(62) Noh, J.; Osman, O. I.; Aziz, S. G.; Winget, P.; Brédas, J.-L. A density functional theory investigation of the electronic structure and spin moments of magnetite. *Sci. Technol. Adv. Mater.* **2014**, *15*, No. 044202.
(63) Zhang, Y.; Sun, J.; Perdew, J. P.; Wu, X. Comparative first-principles studies of prototypical ferroelectric materials by LDA, GGA, and SCAN meta-GGA. *Phys. Rev. B* **2017**, *96*, No. 035143.
(64) Chen, J.; Wu, X.; Selloni, A. Electronic structure and bonding properties of cobalt oxide in the spinel structure. *Phys. Rev. B* **2011**, *83*, 245204.
(65) Bajdich, M.; García-Mota, M.; Vojvodic, A.; Nørskov, J. K.; Bell, A. T. Theoretical investigation of the activity of cobalt oxides for the electrochemical oxidation of water. *J. Am. Chem. Soc.* **2013**, *135*, 13521−13530.
(66) McCloy, J. S.; Jiang, W.; Bennett, W.; Engelhard, M.; Lindemuth, J.; Parmar, N.; Exarhos, G. J. Electrical and Magnetic Properties Modification in Heavy Ion Irradiated Nanograin $Ni_xCo_{(3-x)}O_4$Films. *J. Phys. Chem. C* **2015**, *119*, 22465−22476.
(67) King, W. J.; Tseung, A. C. C. The reduction of oxygen on nickel-cobalt oxides—II: Correlation between crystal structure and activity of Co_2NiO_4 and related oxides. *Electrochim. Acta* **1974**, *19*, 493−498.
(68) Windisch, C. F., Jr.; Ferris, K. F.; Exarhos, G. J. Synthesis and characterization of transparent conducting oxide cobalt−nickel spinel films. *J. Vac. Sci. Technol., A* **2001**, *19*, 1647−1651.
(69) Verma, S.; Kumar, A.; Pravarthana, D.; Deshpande, A.; Ogale, S. B.; Yusuf, S. M. Off-stoichiometric nickel cobaltite nanoparticles: thermal stability, magnetization, and neutron diffraction studies. *J. Phys. Chem. C* **2014**, *118*, 16246−16254.
(70) Nydegger, M. W.; Couderc, G.; Langell, M. A. Surface composition of $Co_xNi_{1-x}O$ solid solutions by X-ray photoelectron and Auger spectroscopies. *Appl. Surf. Sci.* **1999**, *147*, 58−66.
(71) Kim, J.-G.; Pugmire, D. L.; Battaglia, D.; Langell, M. A. Analysis of the $NiCo_2O_4$ spinel surface with Auger and X-ray photoelectron spectroscopy. *Appl. Surf. Sci.* **2000**, *165*, 70−84.
(72) Pandey, P.; Bitla, Y.; Zschornak, M.; Wang, M.; Xu, C.; Grenzer, J.; Meyer, D.-C.; Chin, Y.-Y.; Lin, H.-J.; Chen, C.-T.; Gemming, S.; Helm, M.; Chu, Y.-H.; Zhou, S. Enhancing the magnetic moment of ferrimagnetic $NiCo_2O_4$ via ion irradiation driven oxygen vacancies. *APL Mater.* **2018**, *6*, No. 066109.
(73) Coey, J. M. D.; Venkatesan, M. Half-metallic ferromagnetism: Example of CrO_2. *J. Appl. Phys.* **2002**, *91*, 8345−8350.
(74) Coey, J. M. D.; Sanvito, S. Magnetic semiconductors and half-metals. *J. Phys. D: Appl. Phys.* **2004**, *37*, 988.
(75) Santos-Carballal, D.; Roldan, A.; Grau-Crespo, R.; de Leeuw, N. H. First-principles study of the inversion thermodynamics and electronic structure of FeM_2X_4 (thio) spinels (M=Cr, Mn, Co, Ni;X=O, S). *Phys. Rev. B* **2015**, *91*, 195106.

https://doi.org/10.1021/acsomega.1c00295
ACS Omega XXXX, XXX, XXX−XXX